JOURNAL OF GEOPHYSICAL RESEARCH, VOL. 93, NO. B11, PAGES 13,037–13,045, NOVEMBER 10, 1988

# Borehole Gravity Measurements in the Salton Sea Scientific Drilling Project Well State 2-14

PAUL W. KASAMEYER AND JOSEPH R HEARST

*Lawrence Livermore National Laboratory, Livermore, California*

Borehole gravity measurements over a depth range from 1737 to 1027 m and the vertical gradient of gravity above ground were measured at the Salton Sea Scientific Drilling Project well State 2-14. Uncorrected borehole gravimetric densities match values from gamma-gamma logs, indicating that the high densities seen in State 2-14 in the depth range 0.5–3 km extend for a few kilometers from the well. The aboveground gradient was found to be 4.1 μGal/m higher than expected; correcting for this value increases the gravimetric density in the borehole. Combining the borehole gravity and estimated vertical gravity gradients on the surface, we find that this densified zone coincides with much of a broad thermal anomaly that has been found to the northeast of the Salton Sea geothermal field.

## INTRODUCTION

The Salton Sea Scientific Drilling Project (SSSDP) drilled borehole State 2-14 into the hydrothermal system at the Salton Sea geothermal field (SSGF). *Elders et al.* [1972] described how the Salton Trough was formed over the last 4 m.y. by oblique relative motion between the Pacific and North American plates and identified a number of pull-apart zones where the spreading currently appears to be concentrated. The northernmost pull-apart zone lies under the SSGF, the largest, hottest geothermal system in the Salton Trough. Here, heat and material from the mantle are modifying young sediments and ultimately augmenting the continental crust. The SSSDP provides the opportunity to study the system's thermal and chemical evolution and, ultimately, to learn more about the nature of this process of crustal development.

Density is important for understanding geothermal systems in the Salton Trough [*Muramoto and Elders*, 1984]. The trough is filled with young deltaic sediments, whose density would normally be expected to increase with depth along well-known compaction curves. In the geothermal systems the sediments have undergone substantial alteration and metamorphism; consequently, they are much denser than predicted from compaction curves. Muramoto and Elders used the increase in bulk density with depth for both sand and shales, as well as resistivity logs, to identify zones of increasing thermal alteration with depth in the wells from the SSGF and to infer the maximum temperature seen by the sediments. State 2-14 provides the opportunity to extend these studies with an large set of cores, cuttings, and well logs.

Because density in the Salton Trough is diagnostic of the degree of alteration, it is correlated with temperature. As a result, routine surface gravity surveys [*Biehler et al.*, 1964] have been used to identify potential geothermal fields. This approach is so successful that *Combs* [1971] reports a one-to-one correspondence between gravity anomalies and thermal anomalies in the Imperial Valley. A +20 mGal residual gravity anomaly, inferred to be caused by a combination of altered sediments and possible deeper intrusions [*Biehler et al.*, 1964], is centered on the SSGF. Because of the ambiguity inherent in gravity interpretation, surface measurements cannot distinguish between laterally extensive, near-surface altered sediments and deeper, denser intrusions. Interpretation of the logs and detailed sampling of State 2-14 will provide additional constraints on the density distribution with depth.

State 2-14 lies near the edge of a zone of high heat flow inferred to mark the active convecting portion of the hydrothermal system and therefore might be near the edge of the zone of high-density sediments. A borehole gravity survey was planned to place constraints on the distance to this edge and on the depth distribution of anomalously dense sediments. In this paper we describe the results of that survey and their implications for the thermal history of the SSGF.

## THERMAL STRUCTURE OF THE SALTON SEA GEOTHERMAL FIELD

The temperature distribution in the SSGF is discussed by *Newmark et al.* [this issue] and *Sass et al.* [this issue]. Newmark et al. report on shallow thermal gradient measurements in and surrounding the SSGF and identify areas with four distinct temperature-depth profiles representing the dominance of different mechanisms of thermal transport. The areas are shown in Figure 1. Figure 2*a* shows typical thermal profiles for each area. The largest area (V) covers most of the Imperial Valley, which *Lachenbruch et al.* [1985] recognized has an anomalously high thermal gradient of about 0.07°C/m. Surrounding the SSGF on at least three sides is the Broad (B) anomaly with nearly conductive temperature profiles and a typical gradient of 0.1°C/m. Deep holes have been drilled in two locations identified in Figure 1 as the South Broad (SB) and North Broad (NB) areas. The Central (C) area of the geothermal field is a 4-km-wide swath with a uniformly high surface gradient of about 0.4°C/m. Decreasing gradients at depth imply convective transport in this area. Finally, within the Central area are two localized, intense convective areas (called the Mullet Island anomaly (M) and the Kornbloom Road anomaly (K)), with gradients as high as 0.8°C/m.

State 2-14 lies near the outer boundaries of both the M and C high-gradient areas. *Sass et al.* [this issue] report on thermal measurements in State 2-14, which has an unusually high near-surface gradient, perhaps associated with the M anomaly. Below 150 m, State 2-14 has temperatures intermediate between wells within the C and B areas.



Paper number 88JB03106.
0148-0227/88/88JB-03106$05.00

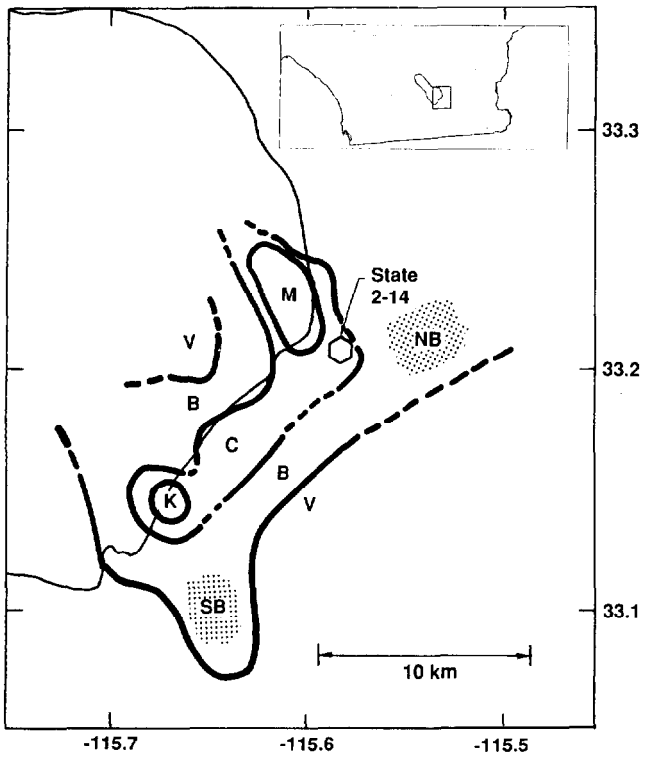


Fig. 1. Thermal zones at the Salton Sea geothermal field. The inset map shows the location of the figure near the Salton Sea and the southern end of the San Andreas fault zone in southern California. The heavy lines indicate the approximate boundaries of thermal regimes defined by *Newmark et al.* [this issue]: V, Valley-Wide; B, Broad; C, Central; and M and K represent two local anomalies, the Mullet Island and Kornbloom Road features. Geothermal data have been published for two portions of the B area indicated by shading: the Westmorland Field, called South Broad (SB) in this paper, and the Niland Field, called North Broad (NB). The smoothed 1959 boundary of the Salton Sea [after *Army Map Service*, 1959] and the approximate location of State 2-14 are also indicated.

## Density Logs From the SSGF Wells

*Muramoto and Elders* [1984] examined the changes in resistivity logs and gamma-gamma density logs with depth in the SSGF to study the mechanisms and distribution of alteration. They developed empirical relationships to infer the degree of hydrothermal alteration from examination of the logs. They concluded that within the C and SB areas, different ranges of shale density are associated with each zone of alteration and therefore each temperature interval. Their conclusions, summarized in Table 1, can be used to estimate temperatures. A shale density of 2.15 is diagnostic of temperatures near 190°C, 2.25 is diagnostic of 240°C, and a rise in shale density to 2.6 is diagnostic of temperature near 295°C. At any depth, densities in the SB anomaly are lower, consistent with the observed lower temperatures.

Figure 2*b* shows idealized shale density profiles based on Muramoto and Elders' data from the northeastern part of the C anomaly and from the SB anomaly. Idealized temperature profiles for these same areas, from *Newmark et al.* [this issue] are shown in Figure 2*a*. Temperature data [*Sass et al.*, this issue] and density data from State 2-14 are also included in Figure 2. The State 2-14 temperatures are lower than those seen in the C anomaly, but the density-depth data are similar.

Using the density-temperature relationship described above, we have calculated the temperatures implied by the density log from State 2-14. Shown as circles in Figure 2*a*, the implied temperatures are higher than the temperatures observed in the well and above 1 km are much closer to the temperature-depth profile for the C area. This observation is consistent with conclusions of *Andes and McKibben* [1987], who inferred that paleotemperatures were 40°–100°C higher than present temperatures based on fluid inclusions from veins in State 2-14, and with *Sturtevant and Williams* [1987], who found that the calcium isotopic profile was similar to that observed in the higher gradient wells in the center of the SSGF.

A similar density-depth relationship is suggested for the NB area. *Muramoto and Elders* [1984] reported Britz 3 density logs, between 200- and 1000-m depth. These logs showed anomalously higher densities than could be predicted from the observed temperature-depth curves, which are similar to those from the SB area. Idealized shale density from the Britz 3 well in the NB area is also shown in Figure 2*b*.

The temperature and density logs show that although State 2-14 is situated off the edge of the central thermal anomaly, its densities are as high as any measured in the SSGF. These high densities suggest that in the past it was as hot as the Central area is now. Since borehole gravity measurements are sensitive to density out to several hundred meters from the borehole, we can estimate how far from State 2-14 the densified area extends by comparing borehole gravity and density logs.

## Measurements in State 2-14

The gamma-gamma density data measured in State 2-14 from 1027 to 1750 m are shown in Figure 3. The gamma-gamma density data were obtained with a standard Schlumberger compensated density log (FDC); the collection and processing of these data are described by *Paillet* [1986]. The tool has two detectors designed to compensate the measured density for gaps between the sonde and borehole wall, as discussed by *Hearst and Nelson* [1985]. The gravimetric density was obtained from a gravimeter survey conducted by EDCON, Inc. in March 1986. The field procedures and analysis are described by *EDCON Inc.* [1986]. Measurements started at a depth of 1737 m, near the bottom of the production casing, and were stopped at 1027 m because of difficulties with the equipment. Forty-six readings were taken with the instrument clamped at 36 different depth stations selected to encompass zones of uniform density as determined from the density log; the results are displayed in Table 2. The gravity data were corrected for drift and tide by standard methods [*EDCON, Inc.*, 1986]; no terrain correction was required at this site. Drift corrections were made by reoccupying stations approximately every half hour and by requiring the gravity readings to agree. Uncertainty of the density, based on the variability of drift-corrected gravity readings, is estimated to vary between 0.001 and 0.007 g/cm$^3$.

The gravimetric density (calculated from equation (4) discussed below) is overlaid on the gamma-gamma density data in Figure 3. The gravimetric density anomaly (the gravimetric density minus the gamma-gamma density data averaged over the interval between gravity measurements) is shown on the left side of Figure 3. Dashed intervals indicate depth intervals where the gamma-gamma data are suspect because the gap and mudcake compensation is greater than 0.07 g/cm$^3$, the maximum value that we consider acceptable.

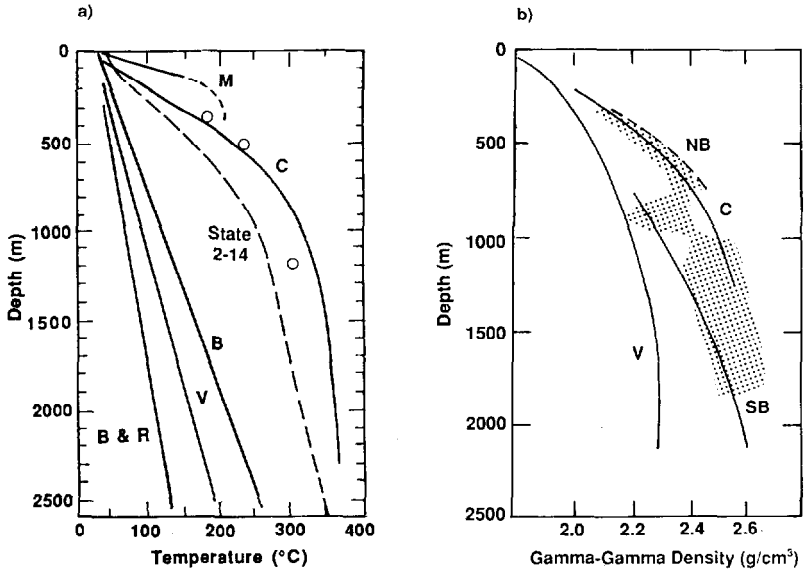


Fig. 2. Idealized (*a*) temperature-depth and (*b*) density-depth profiles for areas defined in Figure 1 and for State 2-14. A typical profile from the Basin and Range (B&R) has been added in Figure 2*a* to show that all the areas described have elevated heat flow. The State 2-14 temperature profile is from *Sass et al.* [this issue], and all others are from *Newmark et al.* [this issue]. The three circles represent temperatures inferred from the density data in State 2-14, as is described in the text. The shaded area in Figure 2*b* represents all density log points with compensation less than 0.07 g/cm$^3$ in State 2-14 [*Paillet*, 1986]; all other profiles are from *Muramoto and Elders* [1984]. The lines represent average shale densities for the SB, NB, and C anomalies and an estimate of the unaltered compaction curves for the V area.

Several details of the log density are matched by the gravimetric density, (e.g., step changes at 1570, 1271, and 1173 m), indicating that the depths of the two measurements were well aligned. The similarity of the offsets on the gravimetric and gamma-gamma density logs can be used to estimate the lateral extent of the small density fluctuations seen in State 2-14. Some of these small zones must extend horizontally a large distance from the borehole. For example, the density log shows an average density increase of about 0.1 g/cm$^3$ between 1569 and 1661 m. On the basis of the mud logs from *Paillet* [1986], this higher-density zone contains less sandstone and siltstone than the material above and below it. Figure 3 shows that the gravimetric density response to this zone is about 90% of the gamma-gamma response. We assume that the high-density zone is a cylinder centered in the borehole and embedded in a material with the density of the zones above it. Using the formula for the density effect of a cylinder [*Hearst et al.*, 1980], we find that to produce a 90% response, the cylinder radius must be greater than 5 times the thickness, or several hundred meters in this case. Some zones may be much smaller in extent. For the sandy zone between 1359 and 1377 m the gravimetric density response is less than 30% of the density log response, indicating that the zone radius could be as small as half the thickness, or less than 10 m.

Throughout the borehole, the gravimetric and log densities match well. Except in the lateral from 1289 to 1338 m, the gravimetric density is slightly higher than the log density, a somewhat surprising result given the high densities seen by the log. The mean gravimetric density anomaly (not including the suspect intervals) is 0.02 g/cm$^3$. This value is near the limit of the density log's systematic uncertainty caused by changes in water content and the presence of unusual temperatures, indicating that the true anomaly could be zero. Consequently, when taken at face value, the borehole gravity data suggest that there is no significant anomaly, that on a large scale, density depends on depth only with no lateral variation and that State 2-14 is far from the density boundary of the SSGF. To evaluate this result and to estimate how close the density boundary might be, we look at the analysis of the borehole gravity in detail.

TABLE 1. Characteristic Densities for Different Metamorphic Zones

| Metamorphic Zone | Transition Temperature, °C | Shale Density, g/cm$^3$ | Sand Density, g/cm$^3$ |
|---|---|---|---|
| Montmorillonite | | <2.05 | 2.00–2.15 |
| | 100–190 | | |
| Illite | | 2.15–2.25 | 2.05–2.20 |
| | 230–250 | | |
| Chlorite | | 2.25–2.6 | 2.20–2.40 |
| | 290–300 | | |
| Feldspar | | 2.25–2.65 | 2.25–2.35 |

## Use of Borehole Gravity to Infer Lateral Changes in Density

A gamma-gamma density log and a borehole gravimeter are often used together to infer lateral changes in density that do not intersect the borehole [*Hearst and Nelson*, 1985]. The interpretation approach is based on the gravity response for an infinite slab of density $\rho$. Above and below the infinite slab the gravity is constant, and the difference in gravity ($\Delta g$) measured at the top and bottom of the slab is given by

$$\Delta g/\Delta z = -4\pi K\rho \qquad (1)$$

where $\Delta z$ is the depth difference for the measurements, $z$ in-

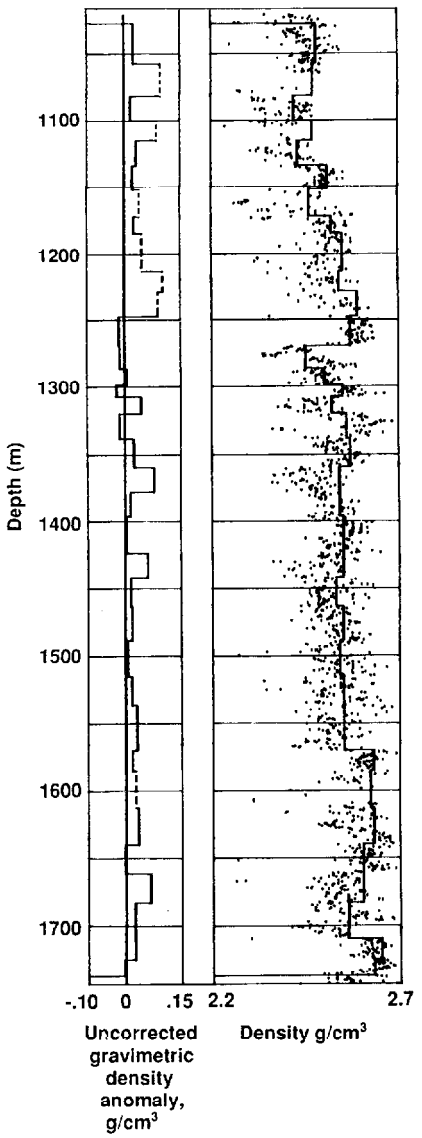


Fig. 3. Gravimetric and gamma-gamma log densities for State 2-14 from 1027 to 1750 m depth. The solid line in the right-hand column is the gravimetric density calculated from equation (4). The density log was sampled every foot, and those points for which the compensation was less than 0.07 g/cm³ are plotted. The uncorrected gravimetric density anomaly, plotted on the left at the same scale, is calculated by subtracting the average of the acceptable density values in an interval from the gravimetric density, as in equation (5). The dashed intervals indicate sections of the density log where the majority of compensation values were greater than 0.07.

creases downward, and $K$ is the gravitational constant. We divide the actual density distribution within the Earth into four components:

$$\rho(x, y, z) = \rho_W(x, y, z) + \rho_L(z) + \rho_A(x, y, z) + \rho_R(x, y, z) \quad (2)$$

where the subscripts have the following meanings:

$W$ rotating oblate spheroid Earth which produces the free-air anomaly $F_W(z)$ given by the formula of *Heiskanen and Vening Meinesz* [1958] with constants given by *Robbins* [1978];

$L$ set of infinite, flat-lying layers passing through the well bore;

$A$ difference between $\rho_L$ and the local anomalous masses that we intend to model, i.e., the "density contrast" of the anomalies;

$R$ regional masses outside the zone that we intend to model.

Following the approach of *Mueller* [1960] (as cited by *Beyer* [1971]) we define regional masses to be those distant enough that their effect on the gradient is constant over the depth of the hole, and we recognize that we must include any closer ones in our local model.

In the following equations, all measurement locations refer to depth within or directly above the borehole, so the $x$ and $y$ parameters are omitted. The measured gravity difference, identified by the superscript $m$, between $z$ and $z + \Delta z$ in the borehole is the sum of the contributions of the four density components:

$$\Delta g^m(z)/\Delta z = F_W - 4\pi K\rho_L + \Delta g_R/\Delta z + \Delta g_A(z)/\Delta z \quad (3)$$

where the contribution from the term representing the layer density has been converted by using equation (1).

If there were no regional and local anomalies, the last two terms on the right-hand side of equation (3) would be zero, and the density-depth distribution could be estimated from the gravity measurements using the standard formula for

TABLE 2. Borehole Gravity Data From State 2-14

| Depth Range, m | Delta $g$, mGal | Gravimetric Density, g/cm³ |
|---|---|---|
| 1027–1057 | 3.086 | 2.48 |
| 1057–1082* | 2.485 | 2.47 |
| 1082–1100 | 1.942 | 2.42 |
| 1100–1115* | 1.554 | 2.47 |
| 1115–1133 | 1.913 | 2.43 |
| 1133–1152 | 1.796 | 2.51 |
| 1152–1171* | 2.032 | 2.46 |
| 1171–1184 | 1.194 | 2.52 |
| 1184–1213* | 2.758 | 2.55 |
| 1213–1228* | 1.458 | 2.54 |
| 1228–1246* | 1.676 | 2.59 |
| 1246–1269 | 2.144 | 2.57 |
| 1269–1286 | 1.736 | 2.45 |
| 1286–1298 | 1.214 | 2.50 |
| 1298–1307 | 0.871 | 2.55 |
| 1307–1319 | 1.194 | 2.52 |
| 1319–1338 | 1.729 | 2.56 |
| 1338–1359 | 2.001 | 2.57 |
| 1359–1377 | 1.756 | 2.54 |
| 1377–1395 | 1.761 | 2.54 |
| 1395–1423 | 2.598 | 2.55 |
| 1423–1441 | 1.737 | 2.55 |
| 1441–1463 | 2.071 | 2.53 |
| 1463–1487 | 2.317 | 2.55 |
| 1487–1514 | 2.639 | 2.54 |
| 1514–1536 | 2.032 | 2.55 |
| 1536–1569 | 3.184 | 2.55 |
| 1569–1584 | 1.349 | 2.63 |
| 1584–1612* | 2.454 | 2.62 |
| 1612–1639 | 2.415 | 2.63 |
| 1639–1661 | 1.944 | 2.60 |
| 1661–1682 | 1.946 | 2.60 |
| 1682–1709 | 2.577 | 2.56 |
| 1709–1725 | 1.327 | 2.65 |
| 1725–1737 | 1.001 | 2.63 |

*Questionable log.

gravimetric density:

$$\rho^m(z) = \frac{1}{4\pi K}\left[F_W(z) - \Delta g^m(z)/\Delta z\right] \quad (4)$$

The density log, $\rho_{LOG}$, measures the density of the hypothetical layers plus the density contrast of any anomalous masses that intersect the borehole. The uncorrected gravimetric density anomaly can be derived from equations (3) and (4):

$$\rho^m(z) - \rho_{LOG} = \rho_A{}^g(z) - \rho_A{}^t(z) + \rho_R{}^g \quad (5)$$

We have divided the gravity gradient terms on the right-hand side of equation (3) by $-4\pi K$ to express them in terms of their density effect $\rho^g(z)$ at depth $z$. The superscript "$g$" is used to distinguish the contribution of a mass to the gravimetric density measured at $x = 0$, $y = 0$ from its true density (indicated by superscript "$t$"). For the infinite layers, $\rho_L{}^t(z) = \rho_L{}^g(z)$, so they do not contribute to the anomaly. We see that the anomalous mass can be detected if its effect on gravimetric density at any depth differs from its density contrast in the borehole at that depth.

In State 2-14 the uncorrected gravimetric density anomaly is small; from equation (5) we see that two cases are possible. In the first case, either there is no anomalous mass that influences the gradient over the depth range studied, or the anomalous mass extends so far from the borehole that it is in effect a layer. In the second case, the anomalous mass produces a uniform gravity gradient that is cancelled by a regional anomaly of opposite sign. As in most gravity problems, if regional effects are not adequately removed, they contaminate the data to be modeled; in this case, the regional masses add a constant to the uncorrected gravimetric density anomaly. One way to remove the effects of regional masses is to subtract the estimated density calculated from the gradient observed above the ground surface, where the density of air can be neglected, from the gravimetric density at depth to get the corrected gravimetric density,

$$d\rho^m(z) = \rho^m(z) - \rho^m(0) \quad (6)$$

and the corrected gravimetric anomaly is again found by subtracting the log density, and using the assumption stated above that the regional vertical gradient is constant,

$$d\rho^m(z) - \rho_{LOG}(z) = \rho_A{}^g(z) - \rho_A{}^t(z) - \rho_A{}^g(0) \quad (7)$$

Equation (7) describes the relationship between measurements and the density distribution:

1. On the right-hand side is the actual anomalous mass, as reflected in its density effect at the surface and at depth and its true density along the borehole.
2. On the left-hand side are the observations, reflected in the density effects of the measured gradients at the surface and at depth, and the well log.

## VERTICAL GRADIENT OF GRAVITY NEAR STATE 2-14

To estimate the corrected gravimetric density anomaly at State 2-14, we found the vertical gradient above the surface by two independent means: by measuring it on the drill rig and by estimating it from gravity measurements on the Earth's surface within 100 km of State 2-14. The gradients obtained by these independent methods agree and produce a slightly positive corrected gravitational anomaly throughout the borehole.

M. R. Millett and D. J. Felske of Lawrence Livermore National Laboratory measured the free-air gradient at this site by occupying gravity stations on the drill rig at heights 8.1 and 32.5 m above ground surface. Their measurements are reported in Table 3. The measured free-air gradient was 312.9 $\mu$Gal/m, 4.1 $\mu$Gal/m more than $F_W$ (which is 308.8 $\mu$Gal/m).

Measured gradients can be disturbed by very local features, such as the mass of the drill rig, mud pits, and subtle local topography [*Beyer*, 1971]. To determine if our measured gradient is disrupted by local features, we used a method described by Beyer to calculate the anomalous free-air gradient from surface gravity measurements surrounding State 2-14. We selected all 7423 values of the simple Bouguer anomaly (corrected with density 2.67 g/cm$^3$) within a 100-km radius of State 2-14 from a data set compiled by the National Oceanographic and Atmospheric Administration (unpublished data, 1982). The vertical gradient was estimated at each of 495 observation points in the rectangle covered by Figure 1. For each point the Bouguer anomaly data were averaged over 20° azimuthal zones within each of 15 distance rings with outer radii covering a geometric series from 1 to 100 km. The average of the filled zones in each ring was used to estimate the average gravity value as a function of distance, and the gradient at the surface due to anomalous and regional masses was calculated using Beyer's equation 14. To ensure adequate azimuthal coverage, we interpolated gravity values over the southeastern end of the Salton Sea.

The simple Bouguer anomaly data around State 2-14 are contoured in Figure 4, and the calculated gradient anomalies are shown in Figure 5. The estimated anomalous vertical gradient at State 2-14 is 4.3 $\mu$Gal/m, within 10% of the measured value, raising our confidence in its applicability.

When we use this measured free-air gradient in equations (4) and (7), the corrected gravimetric density is larger than the uncorrected value by almost 0.05 g/cm$^3$, giving an average anomaly of 0.07 g/cm$^3$, a significant value. Equation (7) shows that this nearly uniform density anomaly could be produced either by a model with a density effect at depth such that $\rho^g(z) > \rho^t(z)$, or one with a negative density effect at the surface.

## MODELING

### *Models That Produce a Positive Density Anomaly at State 2-14*

The observed corrected gravimetric density anamaly of 0.07 g/cm$^3$ is surprising in view of the high densities and high shale content observed in State 2-14 and the expectation that cooler regions surrounding it would have lower density. This anomaly could, in principle, be explained by either of two simple models with $\rho^g(z) > \rho^t(z)$. The first model has infinite horizontal layers with density 0.07 g/cm$^3$ larger than the gamma-gamma density. The observed log values would then be produced by an anomalous mass of $-0.07$ g/cm$^3$ surrounding the borehole. The second model requires the presence of a large amount of high-density material near but not intersecting the borehole. There is no independent geological evidence for higher-density material near the borehole. Possible sources of excess mass include dense intrusions, intense alteration at the M thermal anomaly, and lithologic changes such as a drastic increase in shale content near the borehole.

For a model to be useful, however, it should have some

TABLE 3. Gravity Measurements Above State 2-14 on April 8, 1986

| | Tide Correction, mGal | Corrected Gravity, mGal | |
|---|---|---|---|
| | | 8.11 m | 32.47 m |
| Time LT | | | |
| 0700 | −0.056 | 3357.646 | |
| 0722 | −0.040 | | 3350.040 |
| 0733 | −0.032 | 3357.660 | |
| 0743 | −0.024 | | 3350.035 |
| 0754 | −0.014 | 3357.658 | |
| 0805 | −0.005 | | 3350.036 |
| 0815 | −0.004 | 3357.663 | |
| 0823 | 0.011 | | 3350.046 |
| 0832 | 0.019 | 3357.669 | |
| Average | | 3357.659 | 3350.039 |

Gradient is 7.620 mGal/24.36 m = 312.9 μGal/m.

corroboration from independent observations. We use the surface gravity field for corroboration. Since the surface gravity anomaly contours (Figure 4) are somewhat circular, we restrict our models to cylinders of radius $r_c$ with a vertical axis at the center of the surface gravity anomaly, as shown in Figure 6. We simplify the problem by considering the measured value of the corrected gravimetric density anomaly, the left side of equation (7), to be 0.07 g/cm$^3$ over the depth range 1027–1737 m. Values of the anomaly are calculated along the borehole axis ($r = r_0$), as functions of the cylinder radius $r_c$, using the formulation of *Singh* [1977].

First, we consider the possibility that State 2-14 lies outside of the cylinder ($r_c < r_0$). In Figure 2*b* we see that the density from State 2-14 is very similar to values observed in the central portion of the geothermal field. The highest log values detected in C area, from Magmamax 2 (but incorrectly labeled by *Muramoto and Elders* [1984, Figure 43] as Magmamax 3), are no more than 0.1 g/cm$^3$ greater than the shale densities at State 2-14. To see if higher densities in the C area could cause the borehole gravimetric anomaly, we model this possible high-density anomaly as a cylinder with $r_c < r_0$, top depth $z_1 = 500$ m, bottom depth $z_2 = 3000$ m, and density contrast $\Delta\rho = 0.1$. The curve marked model 1 in Figure 7 shows the depth-averaged corrected gravimetric anomaly that would be seen in State 2-14, as a function of the radius $r_c$ assumed for the cylinder. (Making $z_2$, the depth to the bottom of the cylinder, larger decreases the size of the anomaly.) It appears that excess density in the center of the field can cause a positive anomaly, but not as large as the one observed.

Next, we evaluate the alternative that State 2-14, which has a large proportion of high-density shale, lies within the anomalous mass ($r_c > r_0$). Of course, the outer boundary of this mass would cause a negative gravimetric anomaly, the opposite of that which was detected. But that subsurface mass anomaly also affects the measured free-air gradient, in some cases producing a negative density effect at the surface. If the negative density effect at the surface is larger than the negative effect at depth, a positive corrected gravimetric anomaly will be produced. Lacking constraints from borehole gravity data

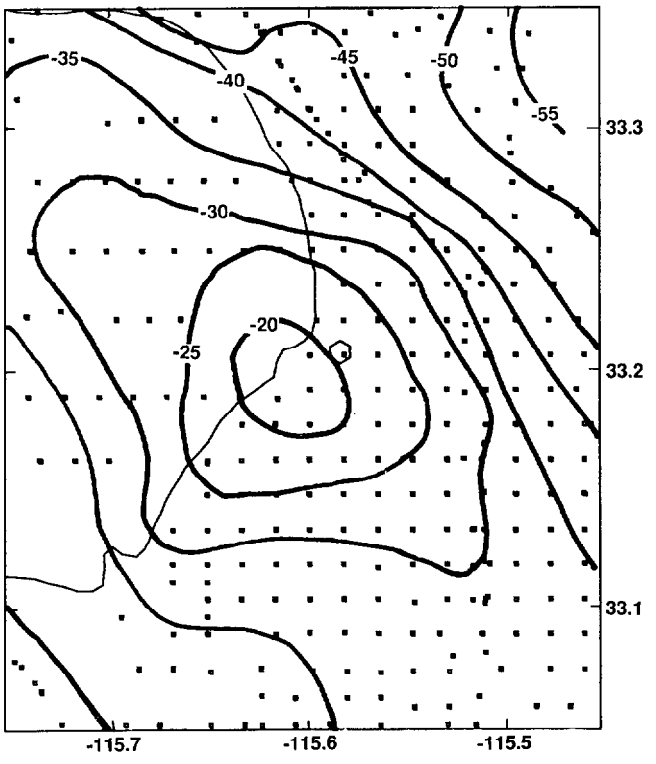


Fig. 4. Gravity data in the area covered by Figure 1. Contours derived from Bouguer corrected observations (using a density of 2.67 g/cm$^3$) near State 2-14, whose location is indicated by a hexagon. The squares represent gravity station locations in the mapped area. The data were obtained from NOAA and are very consistent with the gravity map of *Biehler et al.* [1964]. The contour interval is 5 mGal.

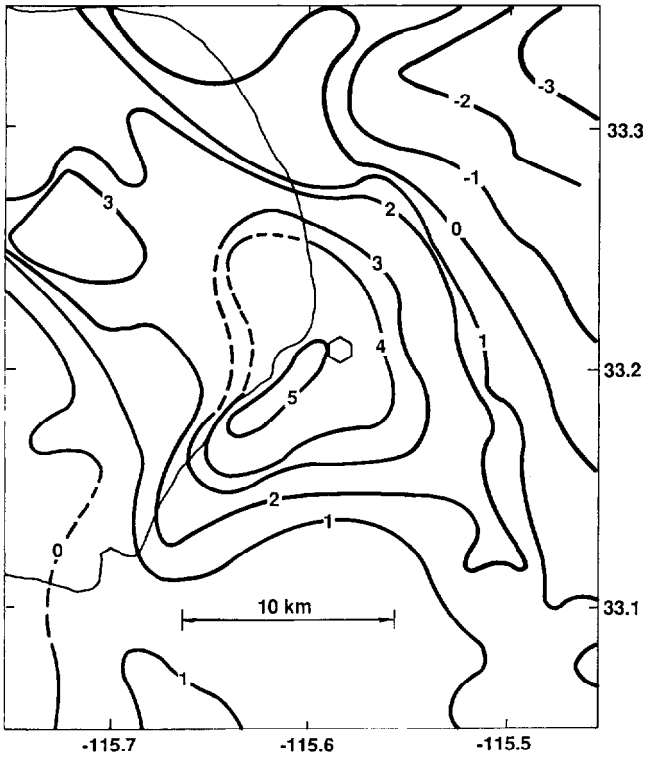


Fig. 5. Anomalous vertical gravity gradients (in microGals per meter) estimated from surface gravity measurements within 100 km of State 2-14, whose location is indicated by a hexagon. Data from a much larger area than is shown in Figure 4 were used to calculate the vertical gradients in Figure 5. The method of calculation is discussed in the text.

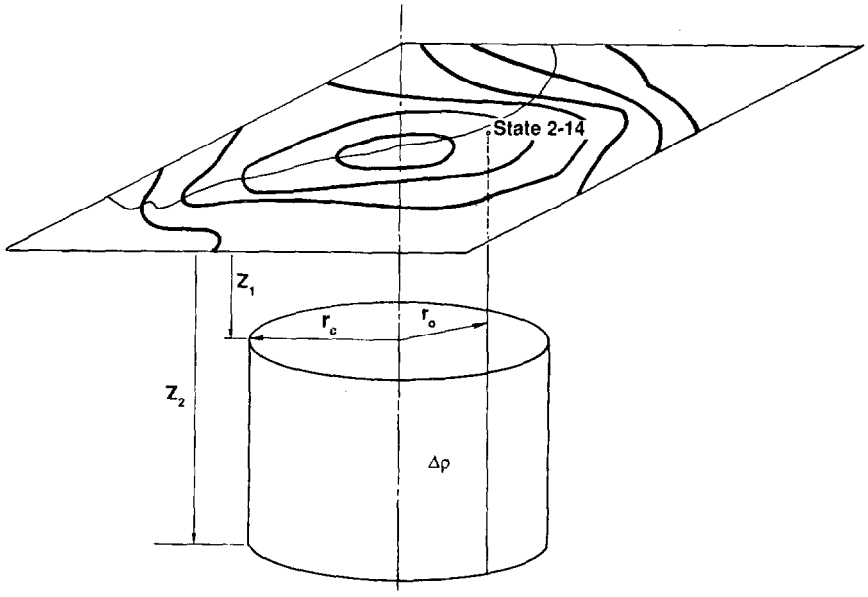


Fig. 6. The gravity model discussed in this paper. A cylinder with a vertical axis is assumed to lie beneath the center of the gravity anomaly. Different values of the parameters $z_1$, $z_2$, $r_c$, and $\Delta\rho$ are discussed in the text. State 2-14 lies at a distance $r_0 = 3962$ m from the center of the axis.

near the surface, we can make only simple models that indicate what is required to fit the data.

Shallow dense cylinders can produce the corrected gravimetric anomaly that was detected. A cylinder with $r_c$ slightly greater than $r_0$ produces an anomalous gradient at the surface. For model 2 we arbitrarily set $\Delta\rho = 0.45$, the largest difference in density between the C and V curves in Figure 2, $z_1 = 50$ m and $z_2 = 500$ m. (If $z_2$ were much larger, this model would

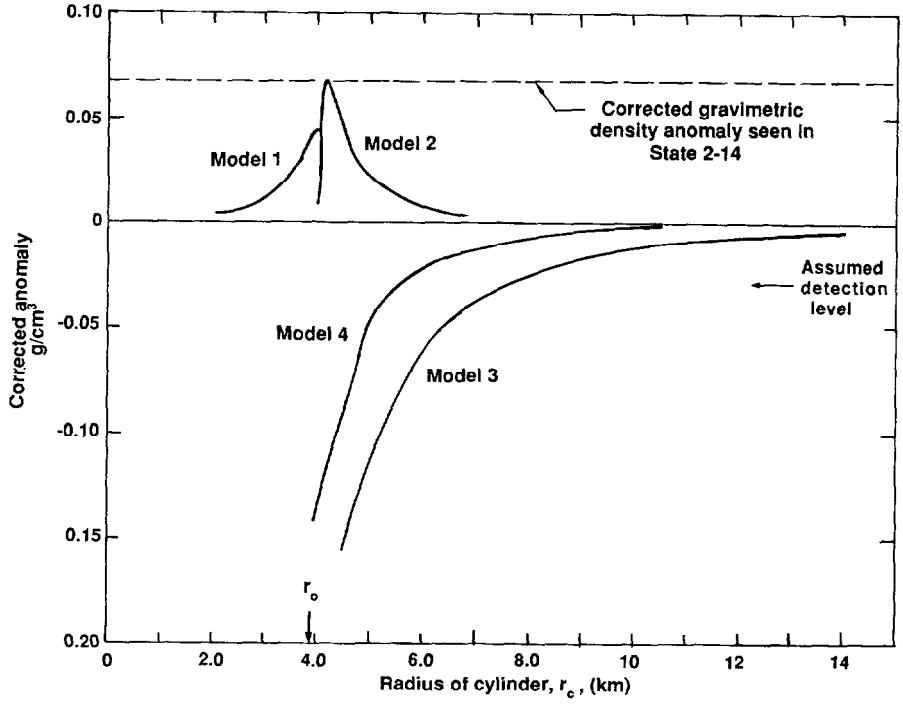


Fig. 7. Calculated corrected gravity anomaly at State 2-14 due to cylindrical models, as a function of the model cylinder radius $r_c$. The arrow at the bottom shows $r_0$, the radius from the center of the cylinder to State 2-14. The corrected anomaly is given by the right-hand side of equation (7), and the model parameters are described in Figure 6. Model 1 has a density contrast of 0.1, corresponding to the largest difference in density between the C area and the density observed at State 2-14, $z_1 = 500$ m and $z_2 = 3000$ m. Model 2, the "shallow" model, has a contrast of 0.45, corresponding to the difference in density between the C area and the average density in the Imperial Valley, $z_1 = 50$ m, and $z_2 = 500$ m. Model 3 has the same density contrast as model 2, but $z_1 = 500$ m, $z_2 = 5000$ m. Model 4 has a contrast of 0.25, corresponding to the difference in density between the C area and the SB area, with $z_1 = 500$ m and $z_2 = 3000$ m. Only the shallow model 2 produces the observed positive anomaly of 0.07 g/cm$^3$.

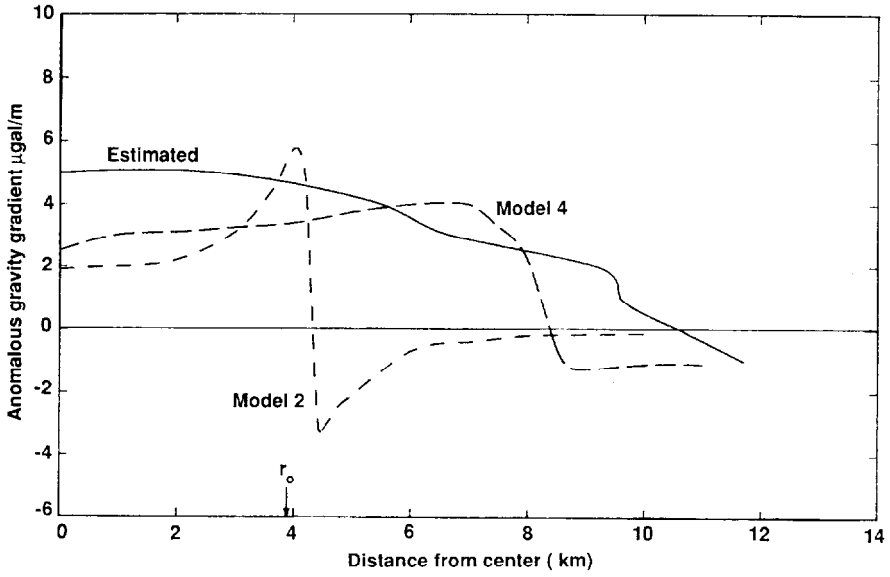


Fig. 8. Estimated vertical gradient anomaly data (from Figure 5) sampled along a northwest trending line from the center of the gravity anomaly, compared to calculated anomalous vertical gradients at the surface, for specific values of the model cylinder radius $r_c$, for models 2 and 4 from Figure 7. All curves are plotted as a function of distance of the measuring point from the center of the cylinder. The arrow at the bottom shows $r_0$, the radius to State 2-14. Model 2 is a shallow cylinder with $r_c = 4300$ m and produces the positive corrected gravimetric density anomaly seen in State 2-14 but does not match the surface observations shown here. Model 4, a deeper cylinder with $r_c = 8$ km, matches the estimated vertical gradient profile along the surface but produces almost no anomaly in the borehole.

cause variations in the anomaly over the depth range where we detected it to be constant.) The curve shown as model 2 in Figure 7 shows that a shallow body with $r_c$ a few hundred meters greater than $r_0$ could produce our observed corrected gravitational anomaly of 0.07 g/cm$^3$. This was the basis of an earlier published claim that we may have detected a shallow edge of the densified zone just east of State 2-14 [*Kasameyer and Hearst*, 1987]. However, all shallow models that produce a high surface gradient at State 2-14 produce very large changes in vertical gradient as a function of distance, inconsistent with the results shown in Figure 5. This rapid change in gradient is illustrated in Figure 8, which shows the estimated anomalous vertical gradients along a northeast trending line from the center of the gravity anomaly obtained from the measured data shown in Figure 5, compared to surface gradient anomaly as a function of distance from the center of the cylinder calculated from two models. For the curve marked model 2 in Figure 8, we have set $r_c$ to be 338 m greater than $r_0$. The change in gradient for this model is much more rapid than that seen in the curve estimated from surface data. Therefore we now reject near-surface features as a means to produce the observed positive corrected gravimetric anomaly and conclude that the positive borehole gravity anomaly indicates that the densely altered zone extends far enough from State 2-14 that its edge was not detected.

### *Models That Indicate Distance From State 2-14 to Edge of Density Anomaly*

Models 3 and 4 indicate that the edge of the densely altered zone would produce a large negative anomaly unless it is far from State 2-14. We calculate corrected gravimetric density anomalous for two types of cylinders as a function of $r_c$. The depths and density contrasts are chosen, based on the log density data in Figure 2, to reflect two different possible views of the density anomaly. In the first view, represented by model 3, we note that the center of the geothermal field (C) has densities about 0.45 g/cm$^3$ above normal compaction curves (V). This contrast, $\Delta\rho = 0.45$, is applied to a cylinder with $z_1 = 500$ m and $z_2 = 5000$ m, starting shallow enough to produce a uniform disturbance over the depths studied in State 2-14 and extending deep into the sedimentary section. In the second view, model 4, we assume that the central anomaly lies within rock of densities similar to those seen in the SB area. It is modeled by a cylinder with $\Delta\rho = 0.25$, $z_1 = 500$ m, and $z_2 = 3000$ m. As their radii vary, these cylinders cause the anomalies shown as models 3 and 4 in Figure 7. Assuming that a negative anomaly of 0.03 g/cm$^3$ would have been detected, model 4 exceeds that limit if $r_c < 5.4$ km (1.4 km beyond State 2-14), and model 3 exceeds it if $r_c < 8$ km (4 km beyond State 2-14). Consequently, we conclude that the inner boundary of the B area is no closer than 1.4 km to State 2-14 and a boundary where densities return to "normal" is no closer than about 4 km to State 2-14.

The borehole gravity data require that material as dense or denser than that found in State 2-14 exists out to a distance of at least a few kilometers at depths from 1 to 2 km. There is a strong suggestion from the vertical gradient anomaly map (Figure 5) that this distance is of the order of 2–6 km, where there is a zone of very rapid decrease in vertical gradient anomaly from about 2.5 $\mu$Gal/m to about $-1$ $\mu$Gal/m. To illustrate this, the surface gradient calculated from model 4 with a fixed cylinder radius $r_c = 8$ km is compared in Figure 8 to the anomalous surface gradient estimated from surface gravity. It is clear that cylindrical models of this type, which have almost no effect on borehole gravity in State 2-14, can produce many features of the estimated vertical gradient. Both have a broad central area with a constant positive anomalous

gradient and fall rapidly through zero. The model falls off more rapidly, suggesting that the actual boundary is less abrupt or deeper. A comparison of Figures 1 and 5 indicates that the most abrupt decrease in the gradient lies to the east of the NB zone, roughly along an extension of the San Andreas fault zone. Thus the high-density zone probably continues to the NB area, where densities are similar to State 2-14.

## CONCLUSIONS AND DISCUSSION

Our borehole gravity measurements indicate that the dense rocks that penetrated between 1- and 2-km depth in State 2-14 must extend several kilometers from the well. We see a slightly positive corrected gravimetric anomaly whose cause is not known. There is no evidence from the borehole gravity data collected to date that the SSSDP well is near the edge of the high-density zone that it penetrates. This conclusion is reinforced by the vertical gravity-gradient anomaly map (Figure 5), which shows a zone of uniform gradient surrounding the SSSDP. The zone of rapid decrease in gradient NE of State 2-14 and the high densities observed in a well from the NB area suggest that the boundary lies about 6 km from the well in that direction, roughly along a line extending south-southeast from the end of the San Andreas fault zone.

Hydrothermal alteration is the accepted cause of the high densities seen in sedimentary rocks in the SSGF. The occurrence of a large area of high densities to the NE of State 2-14 implies that the upper 2 km of the NB thermal area has been as at least as hot in the past as the C zone of the SSGF is today. Our results suggest that the thermal history of this zone is quite different from the history of the SB area, even though the present-day temperatures are similar [*Newmark et al.*, this issue]. From the location of the NB area between the plate boundary, as defined by the San Andreas fault zone, and the locus of present spreading, as defined by the SSGF, we speculate that this shallow dense area represents an earlier locus of spreading similar to the SSGF today. The nearly constant temperature gradient observed in the NB area (Figure 2) suggests that heating at shallow depths ceased long enough ago for the area to return to steady state conduction. The present elevated temperatures could represent the residual heat from that event, or something independent of it. Assuming that the cooling occurred by conduction and using a diffusivity $\alpha$ for compacted sedimentary rocks of the order of 40 $m^2$/yr and a half thickness $L$ of 1500 m for the thermal zone, we estimate its characteristic thermal time $L^2/\alpha$ to be of the order of 60,000 years. More than twice that time would be required to reach steady state conduction. Thus the minimum age of this paleothermal zone is about an order of magnitude greater than ages of 6000 to 20,000 years estimated for the C anomaly of the Salton Sea geothermal field [*Kasameyer et al.*, 1984].

*Acknowledgments.* We appreciate the help and support of Tom Ashcraft, Doug Joiner, Don Wolcott, and Don Farchone of EDCON, Inc., who collected the data; On-site Science Manager John Sass of the U.S. Geological Survey, who ran the show at State 2-14; Al Duba of Lawrence Livermore National Laboratory (LLNL), who stayed up all night with the experiments; and Mel Millett and Don Felske of LLNL-Nevada, who collected the above ground gravity measurements. Support from George Kolstad of the Department of Energy, Office of Basic Energy Sciences, Geosciences Program, made this project possible. Work performed under the auspices of the U.S. Department of Energy by the Lawrence Livermore National Laboratory under contract W-7405-ENG-48. Two reviewers provided comments that led to significant improvements in the paper. Fred Paillet suggested restructuring the paper to make it easier to understand. Shawn Biehler detected a serious mistake in the scales on our original figures and assisted in the clarification of many of our ideas. We appreciate their efforts.

## REFERENCES

Andes, J. P., Jr., and M. A. McKibben, Thermal and chemical history of mineralized fractures in cores from the Salton Sea Scientific Drilling Project (abstract), *Eos Trans. AGU, 68*, 439, 1987.

Army Map Service, Western United States 1:250,000 series, *Map NI 11-9*, U.S. Geol. Surv., Reston, Va., 1959.

Beyer, L. A., The vertical gradient of gravity in vertical and near-vertical boreholes, Ph.D. thesis, Stanford Univ., Stanford, Calif., 1971.

Biehler, S., R. L. Kovach, and C. R. Allen, Geophysical framework of the northern end of Gulf of California structural province, Marine Geology of the Gulf of California, edited by T. H. van Andel and G. G. Shor, Jr., *Mem. Am. Assoc. Pet. Geol., 3*, 126–143, 1964.

Combs, J., Heat flow and geothermal resource estimates for the Imperial Valley, in *Cooperative Geological-Geophysical-Geochemical Investigations of Geothermal Resources in the Imperial Valley Area of California*, edited by R. W. Rex, pp. 5–27, University of California, Riverside, 1971.

EDCON, Inc., State well 2-14 Niland, California, *Rep. UCRL-15945*, Lawrence Livermore Nat. Lab., Livermore, Calif., 1986.

Elders, W. A., R. Rex, T. Meidav, P. T. Robinson, and S. Biehler, Crustal spreading in southern California, *Science, 178*, 15–24, 1972.

Hearst, J. R, and P. H. Nelson, *Well Logging for Physical Properties*, McGraw-Hill, New York, 1985.

Hearst, J. R, J. W. Schmoker, and R. C. Carlson, Effects of terrain on borehole gravity data, *Geophysics, 45*, 234–243, 1980.

Heiskanen, W. A., and F. A. Vening Meinesz, *The Earth and Its Gravity Field*, McGraw-Hill, New York, 1958.

Kasameyer, P. W., and J. R. Hearst, Borehole gravity measurements in the SSSDP (abstract), *Eos Trans. AGU, 68*, 445, 1987.

Kasameyer, P. W., L. W. Younker, and J. M. Hanson, Development and application of a hydrothermal model for the Salton Sea geothermal field, California, *Geol. Soc. Am. Bull., 95*, 1242–1252, 1984.

Lachenbruch, A. H., J. H. Sass, and S. P. Galanis, Jr., Heat flow in southernmost California and the origin of the Salton Trough, *J. Geophys. Res., 90*, 6709–6736, 1985.

Mueller, I. I., The gradients of gravity and their applications in geodesy, Ph.D. thesis, Ohio State Univ., Columbus, 1960.

Muramoto, F. S., and W. A. Elders, Correlation of wireline log characteristics with hydrothermal alteration and other reservoir properties of the Salton Sea and Westmorland geothermal fields, Imperial Valley, California, USA, *Los Alamos Natl. Lab. Rep., LA-10128-MS*, 1984.

Newmark, R. L., P. W. Kasameyer, and L. W. Younker, Shallow Drilling in the Salton Sea region:, The thermal anomaly *J. Geophys. Res.*, this issue.

Paillet, F. L., (Ed.), Preliminary report on geophysical well-logging activity on the Salton Sea Scientific Drilling Project, Imperial Valley, California, *U.S. Geol. Surv. Open File Rep., 86-544*, 1986.

Robbins, S. L., Re-examination of the values used as constants in calculating rock density from borehole gravity data, *Geophysics, 46*, 208–210, 1978.

Sass, J. H., S. S. Priest, L. E. Duda, C. C. Carson, J. D. Hendricks, and L. C. Robinson, Thermal regime of the State 2-14 well, Salton Sea Scientific Drilling Project, *J. Geophys. Res.*, this issue.

Singh, S. K., Gravitational attraction of a vertical right circular cylinder, *Geophys. J. R. Astron. Soc., 50*, 243–246, 1977.

Sturtevant, R. G., and A. F. Williams, Oxygen isotopic profiles for the State 2-14 geothermal well: Evidence for a complex thermal history, (abstract), *Eos Trans. AGU, 68*, 445, 1987.

J. R Hearst and P. W. Kasameyer, Mail Stop L-209, Energy Program, Lawrence Livermore National Laboratory, P. O. Box 808, Livermore, CA 94550.

(Received September 30, 1987;
revised April 12, 1988;
accepted May 25, 1988.)